Hindawi
Geofluids
Volume 2021, Article ID 6634513, 10 pages
https://doi.org/10.1155/2021/6634513

Research Article

Groundwater Inrush Control and Parameters Optimization of Curtain Grouting Reinforcement for the Jingzhai Tunnel

Gan Li,[1] **Weibin Ma**,[2] **Siming Tian**,[3] **Zhou Hongbo**,[4] **Fan Huabin**,[5] **and Wenhao Zou**[2]

[1]*State Key Laboratory of Hydroscience and Engineering, Tsinghua University, Beijing 100084, China*
[2]*China Academy of Railway Sciences, Railway Construction Research Institute of China Academy of Railway Sciences Group Co., Ltd, Beijing 100084, China*
[3]*China Railway Economic and Planning Research Institute, Beijing 100084, China*
[4]*Nonferrous Geological Exploration and Research Institute Limited liability company, Shenyang 110013, China*
[5]*Jiaoke Transport Consultants Ltd., Beijing 100084, China*

Correspondence should be addressed to Weibin Ma; maweibin_tiekeyuan@163.com

Received 3 December 2020; Revised 17 December 2020; Accepted 24 December 2020; Published 9 January 2021

Academic Editor: Feng Xiong

Based on the systematic study on the characteristics of water and mud inrush during the excavation of Jingzhai tunnel, the mechanism of water inrush seepage transformation caused by excavation disturbance is analyzed. By means of electromagnetic geophysical prospecting, the potential water bearing area of the tunnel was analyzed. The constitutive model of rock mass and grouting parameters are considered in the numerical simulation. The law of tunnel crack initiation and expansion under different curtain grouting parameters is proposed. The characteristics of seepage water inrush caused by excavation are described. It is considered that there are three stages in the seepage characteristics of tunnel: incubation, sudden, and stable. Numerical simulation was used to analyze the crack propagation track and water inflow characteristics under the grouting thickness of 3 m, 5 m, and 7 m. When the curtain grouting thickness was 3 m, the fracture field penetrated the curtain grouting area. The dominant seepage channel is formed, which greatly increases the probability of water inrush. When the curtain thickness is 5~7 m, the expansion of the crack zone can be controlled basically, so that the fracture and water bearing rock layer cannot form a seepage channel. At last, the grouting scheme of 6 m thick grouting and 20 m advanced grouting was selected, and the water seepage was reduced by 83%.

1. Introduction

With the transfer of China's tunnel construction to the central and western regions, especially in the southwest region, the geological structure is complex, the lithology is poor, and the groundwater is rich, which brings a severe test to the engineering construction. Based on the investigation and analysis of water inrush and mud inrush cases, it is found that the water rich fault fracture zone is a common geological structure that causes water and mud inrush. At the same time, excavation disturbance is also the main cause of this kind of disaster. At present, many scholars have carried out a series of research on the evolution mechanism of water inrush and mud inrush in fault fracture zone tunnels. The quantitative research on the parameters of grouting control measures such as curtain grouting is also rich.

For example, Shao et al. [1] established an evolution model of seepage characteristics with multifield coupling. The model is used to study the evolution process of water inrush in fault and the influence of water pressure, initial effective porosity, and initial permeability on water flow. Sun et al. [2] used the COMSOL numerical simulation to analyze the formation and evolution of water inrush channels in deep underground fault mines. The results show that with the advance of the working face, the stress gradually concentrates near the hidden fault. The velocity inside the fault is

much higher than that in the floor, which means that the buried structure is very important for lifting the confined water and destroying the floor. When the failure area is connected with the fracture of the hidden fault, a water injection channel is formed. Liu et al. [3] established the thermal nonlinear hydraulic mechanical coupling model of fault water inrush, studied the water-rock-water interaction, and predicted the fault water inrush. The governing equations of coupled THM model are established by coupling particle transport equation, nonlinear flow equation, mechanical equation, and heat transfer equation. The results show that the mining stress and water flow velocity have great influence for fault zone. Zhou et al. and Wang et al. [4, 5] thought that the fault activity is generally caused by the stress concentration at the fault tip and established a typical calculation model of underground stope with hidden faults. The fault tip field is quantitatively evaluated, the possibility of fault activation is evaluated, and the stress intensity factor reflecting the degree of stress concentration is obtained. Hu et al. and Zhen et al. [6, 7] established a simplified mechanical model including many factors related to the activation and evolution of concealed water conducting faults. The influence of normal stress and shear stress on fault activation and effective shear stress distribution in fault plane are obtained. The factors affecting fault activation include buried depth of buried fault, friction angle of fault surface, advancing direction of working face, and pore water pressure. In order to evaluate the risk of water inrush, AHP and GIS are combined to put forward the vulnerability index method. Six factors controlling the water inrush are analyzed [8–11]. The dynamic process of inrush is reproduced by numerical simulation. The coupling evolution process of stress field, displacement field, and seepage field is analyzed, and the characteristics of precursor information are summarized [12–16]. Liu et al. [17] proposed a seepage erosion-coupled water inrush model to study the seepage erosion characteristics. Based on the classical theory of solute transport, a hydrodynamic model of porous media is proposed. In this model, the change of porosity relates the permeability to the accumulation of particle loss in the seepage erosion process. The influence of curtain grouting thickness on seepage erosion process is studied by using the seepage erosion coupling model. The results show that with the increase of thickness, the seepage erosion process gradually weakens.

Li et al. [18] reviewed the current situation of water and mud inrush prevention and control at home and abroad and introduced the latest development of relevant theories, grouting equipment, and key technologies. According to the constitutive relation of typical fast setting slurry, the time-varying equation of slurry viscosity at different volume ratios is obtained. Zhang et al. [19] proposed the key-hole grouting method and applied it to the treatment of high-pressure water inrush in fractured rock mass. Jiang et al. and Liu et al. [20, 21] established a simplified model to simulate the whole process of water inrush and carried out a series of large-scale geomechanical model tests. The influence of formation pressure, water pressure, and thickness of waterproof board on water inrush is studied. Saleh et al. and Liang et al. [22, 23] investigated the chemical composition of polyurethane and other chemical grouting materials and discussed the grouting methods, grouting materials, advantages and disadvantages, and the application in the field and laboratory. Xu et al. [24] developed a complete set of physical simulation system to study the grouting of high-pressure fissures in deep underground rocks such as deep coal mines. In order to improve the sealing efficiency and dynamic flow resistance of cement slurry, Yang et al. [25] added carbon fiber into cement slurry to develop a new type of flowing water environment slurry. Li et al. [26] simulated the radial transient flow of variable density polymer slurry in a plane fracture. The flow of polymer slurry mainly depends on the secondary pressurization caused by its own expansion, which is different from the diffusion mechanism of constant pressure driven equal density slurry. In order to improve the early strength and grouting effect of flowing water-grouting slurry, Li et al. [27] mixed nano-calcium carbonate and fly ash into cement-based slurry. Through a series of physical simulation experiments, the viscosity test results show that the viscosity of the slurry decreases with the increase of nano-calcium carbonate content. The results show that with the increase of yield stress, consistency index, and flow index, the expansion rate of cement slurry decreases. The nonuniformity of fracture pore size has an important influence on its propagation process [28].

It can be seen from previous research results that many water inrush prevention and control work is in the exploration of continuous progress. Because of the great difference of disaster pregnant mode under different karst environment conditions, different expert teams pay attention to different points, so the research on comprehensive prevention and control measures of tunnel water inrush disaster under complex karst environment conditions is worthy of further study. In view of the phenomenon of crack propagation caused by excavation, the law of crack propagation under different grouting thickness is analyzed in this paper. According to the fracture development law and seepage flow, the appropriate grouting parameters are determined and finally applied to the engineering practice.

2. Background of the Jingzhai Tunnel

2.1. Geological Conditions. Jingzhai tunnel is located on the middle line of Pan Asian Railway from Kunming to Bangkok, which is the administrative region of Jinghong City in Yunnan Province, as shown in Figure 1. This item is a single-track railway tunnel with a cross-section width and height of 10.05 m and 8.16 m, respectively. The tunnel entrance mileage is DK405+615, the exit mileage is DK415+124, the total length is 9509 m, and the maximum buried depth of construction tunnel is 711 m. The surface water and groundwater of the tunnel are relatively developed, and the groundwater is mainly bedrock fissure water and karst water. The normal water inflow of the tunnel is 44100 m^3/d, and the maximum water inflow in rainy season is 66150 m^3/d. In the original project construction scheme, the New Austrian Tunneling Method (NATM) and three-step excavation were adopted. In the process of tunnel construction, serious adverse geological conditions were encountered, and three

Figure 1: Location of Jingzhai tunnel.

outburst events occurred. At present, the remaining work is about to cross the Manmo Xiaozhai-Jiabutuo fault. It is necessary to take prereinforcement measures to ensure the construction safety in the process of crossing the fault. Curtain grouting technology is adopted for prereinforcement.

The tunnel site is located in the middle and low mountains. The underlying bedrock of the tunnel is sandstone, slate with shale, limestone, mudstone, siltstone and coal line, basalt, and dacite porphyry. There are strong tectonic movements in the tunnel site, including Guanhan syncline and Manmo Xiaozhai-Jiabutuo. The axis of Guanhan syncline is about N22°W, and it intersects with the line at about 61° and is supposed to intersect with the tunnel body at DK414+440+490. The Manmo Xiaozhai-Jiabutuo fault strikes N10° to 30°W, and its angle with the line is about 58° and intersects with the tunnel body at DK409+180~+200, which is a compressive reverse fault. The strike of the strata is generally parallel to the fault line. The width of the fault fracture zone is about 20 m. The fault breccia is mainly composed of breccia and mudstone with a small amount of mylonite.

2.2. Analysis of Survey Results by Magnetotelluric Method. The principle of audio frequency magnetotelluric method (AMT) is based on the principle of magnetotelluric sounding (MT). The apparent resistivity frequency curve is used to obtain the distribution of underground resistivity, so as to distinguish lithology and structural bodies, and identify the spatial distribution and properties of underground geological bodies. In this survey, V8 magnetotelluric instrument is used, the transmitting and receiving distance is 12000 m, and the transmitting dipole distance is 1500 m. The receiving dipole distance is 40 m, the point distance is 40 m, the working frequency is 1 Hz-8192 Hz, and the transmitting current is not less than 3 A in high-frequency band and 16 A in medium- and low-frequency band. The Mtsoft 2D magnetotelluric two-dimensional processing and interpretation software is used for processing and interpretation. The original data are preprocessed by overlapping time series, manually selecting time series, robust processing, and other methods, so as to highlight the useful signals, suppress the interference, and improve the signal-to-noise ratio of the data. After preprocessing, the data are processed by denoising, static correction, and spatial filtering, and then one-dimensional and two-dimensional inversions are carried out. According to the resistivity values, the low-resistivity anomalies can be roughly divided into four types: I (more than 2500 Ω M), II (1000~2500 Ω M), III (200~1000 Ω M), and IV (less than 200 Ω M). They are relatively complete rock mass, relatively broken rock mass, weak or water-bearing rock mass, and extremely weak or water-rich rock mass. As shown in Figure 2, the results of comprehensive geophysical and electrical geological section are drawn. On this basis, a comprehensive interpretation of the geological structure and lithology of the tunnel survey line section is made. The surface-weathering layer in the survey area corresponds to the low resistivity characteristics of electrical structure.

The resistivity of DK408+900~DK409+700 section shows very low characteristics, which is strip reflection, and the inversion resistivity gradient value nearby is large, corresponding to the fault fracture zone. It is inferred that the area is Manmo Xiaozhai-Jiabutuo fault. The resistivity of DK410+100~DK410+300 section shows low characteristics, which indicates that the area is a fold structure. The resistance value of surrounding rock of tunnel body is below 2200 Ω M, so attention should be paid to prevent water gushing, mud bursting, and collapse during construction.

2.3. Geological Disasters and Countermeasures. During the construction of DK408+900~DK410+300 section with low resistivity, three water inrush, mud inrush disasters, and

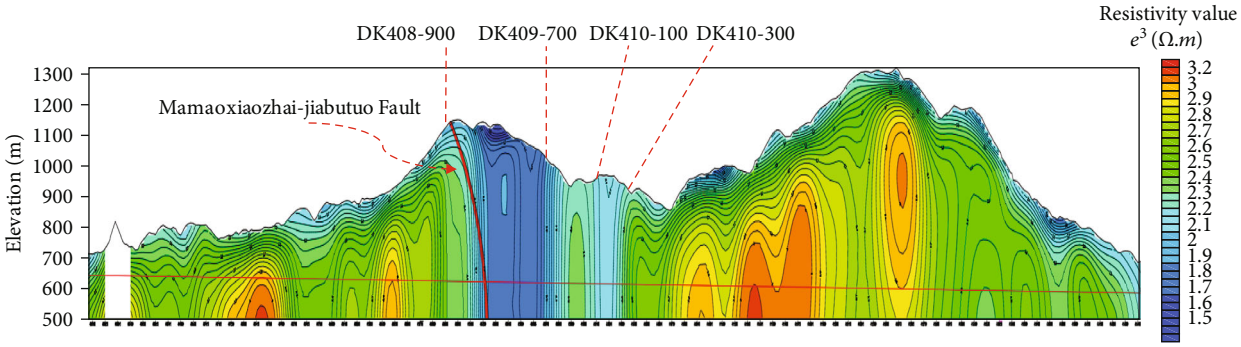

Figure 2: Magnetotelluric inversion results.

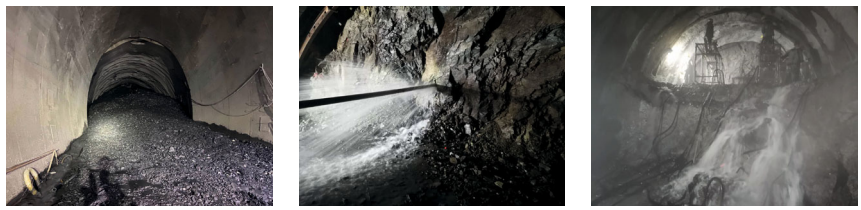

(a) (b) (c)

Figure 3: Water gushing and mud inrush in tunnels. (a) Mud inrush in tunnel. (b) Water inrush from advance probe hole. (c) Tunnel water gushing.

shutdown accidents occurred. Some water and mud inrush photos are shown in Figure 3. The total amount of groundwater and mud is more than 190000 m^3 and 3000 m^3, respectively, and the water pressure is as high as 0.3 MPa. The disaster caused 96 days of construction stagnation and large deformation of surrounding rock. In the construction process, in view of the actual problems such as water gushing and mud bursting, the full-section curtain-grouting technology is proposed. This technology can effectively reduce the water pressure of the water bearing geological body ahead and strengthen and improve the rock mass to prevent the formation of water seepage channel, so as to ensure the safety of tunnel construction. The key indexes of this method are the length of longitudinal grouting reinforcement and the range of circumferential reinforcement.

3. Optimization on the Safety Thickness for the Tunnel

3.1. Tunnel Seepage and Constitutive Model of Rock Mass. In order to simulate the nonlinear dynamic behaviors of water inrush and mud inrush during the construction of carbonaceous slate tunnel, based on the discrete element method and cubic law theory, a coupling model of excavation disturbance crack propagation seepage was established. The model is based on the assumption that primary joints and secondary joints are the dominant seepage channels of tunnels with well-developed fracture fields.

In the process of tunnel excavation and advance, the development of surrounding rock fracture field is a continuous expansion, and when the fracture field intersects with the tunnel water rich area, the water gushing channel will be generated. Under the influence of water, the strength of the surrounding rock decreases sharply, which leads to large-scale deformation of rock mass and influx into tunnel space. Therefore, the most important thing to distinguish the grouting area is to study the development and evolution law of fracture field under different grouting parameters.

3.1.1. Constitutive Model of Rock Mass. The Hoek Brown criterion [29, 30] comprehensively considers the influence of rock mass structure, rock mass strength, and mining in rock mass failure analysis, which makes up for the deficiency of the Mohr Coulomb criterion in rock mass failure analysis to a certain extent. Therefore, the Hoek Brown model is used to study the deformation characteristics and behavior of rock mass. The calculation method is shown in formulas (1) and (2).

$$\sigma_1 = \sigma_3 + \sigma_c(\mathrm{m}_b\sigma_3/\sigma_c + s)^a, \tag{1}$$

$$\left.\begin{aligned} m_b &= m_i \exp\left(\frac{GSI - 100}{28 - 14D}\right) \\ s &= \exp\left(\frac{GSI - 100}{9 - 3D}\right) \\ a &= \frac{1}{2} + \frac{1}{6}\left(\mathrm{e}^{-GSI/15} - \mathrm{e}^{-20/3}\right) \end{aligned}\right\}. \tag{2}$$

In the formula, GSI is the geological strength index, m_i is the rock material index, D is the impact index of blasting

Table 1: Shear strength parameters of slurry rock interface.

Elastic shear modulus G/MPa	Yield stress τ_s/KPa	Peak intensity τ_m/KPa	Residual shear strength τ_t/KPa	Shear stiffness $K_e/(\mathrm{kN\,mm^{-1}})$	Cohesion c/KPa	Internal friction angle φ°	Peak friction coefficient f	Residual friction coefficient f'
5.12	231	332.91	331.27	0.119	96.22	33.3	0.582	0.576

damage on rock mass, m_b, s, and a are the empirical parameters of H-B criterion.

3.1.2. Coulomb Slip Joint Model. The failure modes of joints are mainly shear failure, tension fracture failure, compression shear failure, and tension shear failure. These failure modes can be simulated and analyzed by the Coulomb slip joint model. The calculation principle is as follows [31, 32]:

$$\begin{aligned} F^n &= f^n - k_n \Delta U^n A_c, \\ F_i^n &= f_i^n - k_n \Delta U_i^n A_c. \end{aligned} \tag{3}$$

In the formula, k_n, k_s is the normal stiffness and tangential stiffness of the joint surface; ΔU^n, ΔU_i^n are the contact normal and tangent displacement increments, respectively; and A_c is the contact area.

When the joint is in the elastic stage and there is no slip, the maximum tensile force and shear force on the joint surface are as follows:

$$\begin{aligned} T_{\max} &= -TA_c, \\ F_{\max}^s &= cA_c + F^n \tan\varphi. \end{aligned} \tag{4}$$

In the formula, T is the tensile strength of the joint, and C is the cohesion of the joint.

The cohesion and tensile strength of the joint surface decrease to 0, when the joint is subjected to tensile or shear failure. At this time, the maximum tensile strength of the joint is 0, and the maximum shear strength is $F^n \tan\varphi$.

3.1.3. Cubic Law of Seepage. If the fracture width between the two blocks is a, the relationship between the flow through the fracture q and the fracture width a is as follows:

$$q = \frac{ga^3}{12v} J. \tag{5}$$

In the formula, q is the flow rate (m^2/s), g is the gravity acceleration (m/s^2), a is the fracture width (m), J is the hydraulic gradient, and v is the viscosity coefficient of fluid movement (m/s^2).

According to the formula, the water flow through the fracture is directly proportional to the cubic power of the crack width.

3.2. Grouting Materials. In Jingzhai tunnel, curtain grouting was carried out with cement water glass double-liquid grouting material. The concentration of sodium silicate is 30-35° B é, and volume ratio of cement and water glass is 3 : 1. The strength characteristics of the interface between grout and rock are shown in Table 1.

3.3. Problem Description and Model Setup. The advanced distance and grouting radius of deep-hole grouting are the key parameters to prevent water and mud inrush disasters in water-rich areas. Through the 3DEC numerical simulation software, the development law of fracture field in Jingzhai tunnel is studied by using the treatment method of equivalent joints, and the disaster mechanism of water and mud inrush is revealed. Using the above constitutive model and seepage model, the evolution law of tunnel seepage channel and water inrush characteristics under different safe thickness are simulated. The size of the model is 40 m × 40 m, the simulation strategy of uniformly distributed joints is adopted, and the joint length is 0.3 m as shown in Figure 4.

According to the results of in situ stress test, the vertical principal stress is 13 MPa, the maximum horizontal principal stress is 15 MPa (parallel to the tunnel strike), and the minimum horizontal principal stress is 6 MPa, which is perpendicular to the tunnel strike. The study stratum is mainly carbonaceous slate. Seepage monitoring point A is set at the boundary of the tunnel. It should be noted that the joint surface parameters of the grouting area are different from those of surrounding rock. Under the action of grouting, the joint parameters will be significantly improved. The permeability is related to the original fracture width and the disturbed fracture width.

The seepage boundary is hydrostatic pressure, and 30 m head pressure is applied on the top of the model. The tunnel excavation face is set as a free surface boundary, on which the water flows freely. The relevant parameters used in numerical calculation are shown in Table 2. When the fracture does not contact with the water bearing rock layer, water propagates through the pores, and the relevant permeability parameters are shown in Table 3.

3.4. Result Analysis. On the premise of the advance grouting distance of 20 m, three working conditions of safety thickness of 3 m, 5 m, and 7 m are set, respectively. Numerical simulation was carried out, and the attention duration of each working condition was set as 12 h. There was a detailed analysis, in each case of crack propagation, as well as water inflow.

As shown in Figure 5(a), when the safe thickness is 3 m, the maximum settlement of tunnel vault is 0.19 m. There are many layer separation phenomena above the tunnel. Under the influence of tunnel excavation disturbance, the cracks of tunnel surrounding rocks are produced. The initiation of cracks will produce a dominant flow channel. Under the influence of water pressure, water flows into the tunnel through cracks. As shown in Figure 5(b), the fracture development passes through the safe thickness range of the grouting area, and the top exceeds the grouting boundary by 1.35 m. The bottom is 0.6 m beyond the grouting boundary.

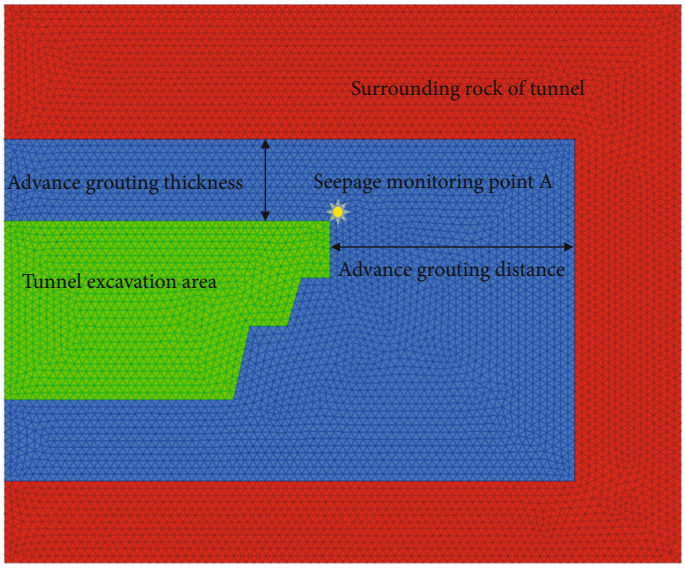

Figure 4: Numerical model of grouting geometric parameters.

Table 2: Mechanical parameters.

Lithology	Rock mass parameters						Joint parameters			
	Density (kg/m^3)	K (GPa)	G (GPa)	C^b (MPa)	φ^b	$\sigma^b{}_t$ (MPa)	K^n (MPa)	k^s (MPa)	C^j (KPa)	φ^j
Carbonaceous slate	2550	13.3	8.4	13.3	31	2.2	2.31	0.56	42.11	23
Grouting carbonaceous slate	2550	13.3	8.4	13.3	31	2.2	5.12	1.27	96.22	33

Table 3: Pore permeability parameters.

Permeability coefficient in carbonaceous slate	5.2×10^{-6} m/s
Permeability coefficient in grouting zone	4.8×10^{-7} m/s
Porosity in carbonaceous slate	0.33
Porosity in grouting zone	0.15
Coefficient	4.2 m^{-1}

At the same time, the fracture developed ahead of the tunnel face, and the lead distance was about 2.8 m. It can be considered that when the safe thickness is 3 m, it cannot meet the requirements of tunnel construction, and water inrush and mud inrush are easy to occur in the construction process.

As shown in Figure 6(a), when the safety thickness is 5 m, the maximum settlement of tunnel vault is 0.1 m. The disturbance range caused by excavation is significantly smaller than that in condition (1). Tunnel separation occurs in the shallow surrounding rock. As shown in Figure 6(b), the fracture development has two dimensions of advance and circumferential. The fracture development is 1.2 m ahead of the working face. The circumferential development of fractures does not cross the grouting area. The depth of the top crack is 1.1 m away from the grouting boundary. The distance between the deepest part of the crack and the grouting boundary is 1.3 m. The water rich rock layer itself has a certain permeability, and even after grouting, there is a certain amount of permeability in the grouting area. However, the risk of water inrush is small, especially when the grouting area is stable and the protective shell is formed.

As shown in Figure 7(a), when the safety thickness is 7 m, the maximum settlement of tunnel vault is 0.07 m. At this time, the development of fracture zone is similar to the safe thickness of 5 m.

As shown in Figure 8, the curve shows the change of seepage flow with time at point a. When the grouting thickness is 3 m, the water inflow does not increase greatly in 0-6 h, but increases rapidly after 6 h. The volume size of monitoring point A is 0.5 m × 0.5 m × 0.5 m, and the final hourly flow rate reaches 12.8 m^3/h. It shows that when the grouting thickness is 3 m, it cannot meet the construction requirements, and there is a greater safety risk. When the grouting thickness is 5 m, the water inflow increases slightly with the increase of time. When the final monitoring point flow increases to 1.8 m^3/h, it tends to be stable. When the grouting thickness is 7 m, the water inflow is basically stable and finally maintained at 0.7 m^3/h. Considering the construction cost and the effect of seepage control, the grouting thickness should be within 5-7 m.

4. Engineering Application

The full-face advanced grouting technology is generally used to detect the situation of large water inflow or poor geological conditions in front of the water exploration hole. After drilling for water exploration, the water yield of each hole shall be measured. When the total water output of 6 holes is more than 5 m^3/h, the construction shall be carried out according to the design drawing of full-section advance pregrouting.

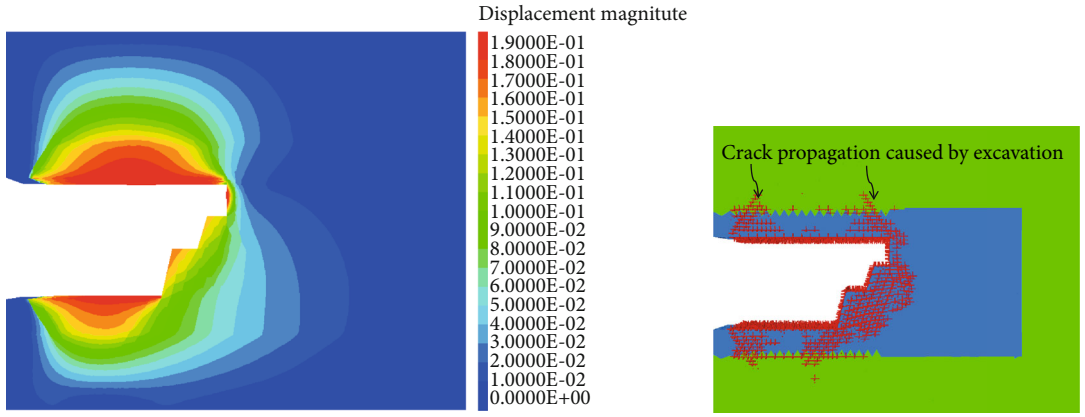

Figure 5: Tunnel displacement and crack propagation when safety thickness is 3 m. (a) Displacement nephogram. (b) Fracture field distribution.

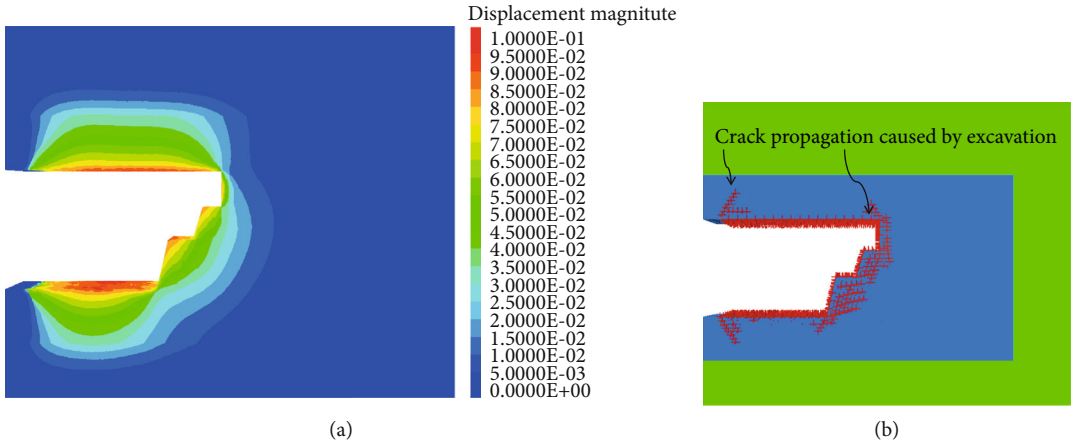

Figure 6: Tunnel displacement and crack propagation when safety thickness is 5 m. (a) Displacement nephogram. (b) Fracture field distribution.

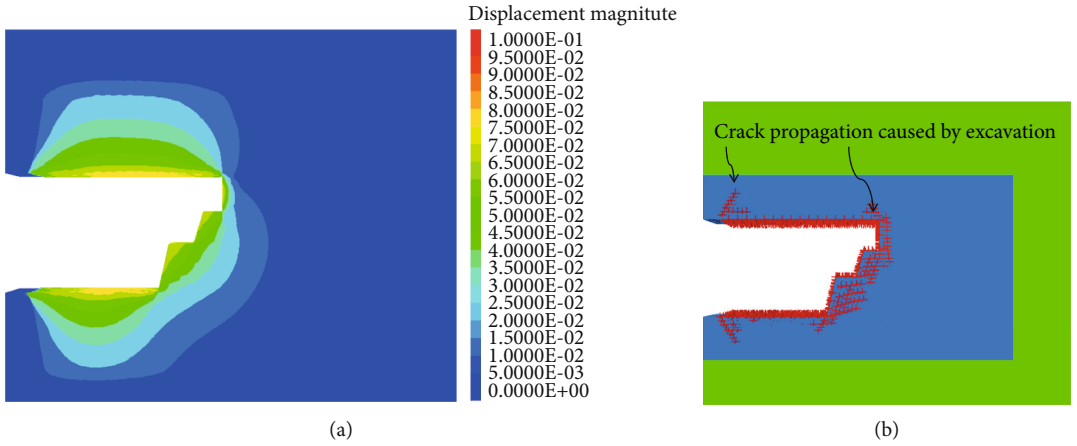

Figure 7: Tunnel displacement and crack propagation when safety thickness is 7 m. (a) Displacement nephogram. (b) Fracture field distribution.

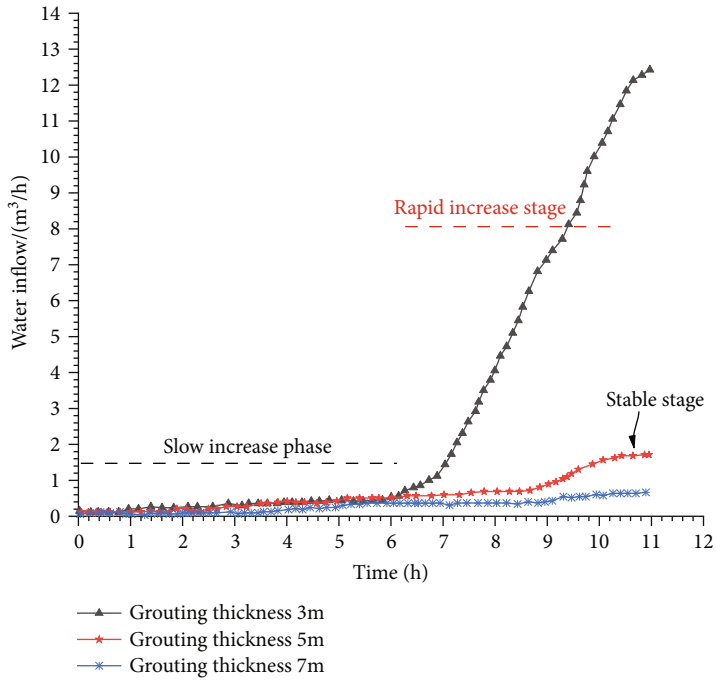

Figure 8: Evolution of water inflow in different grouting thicknesses.

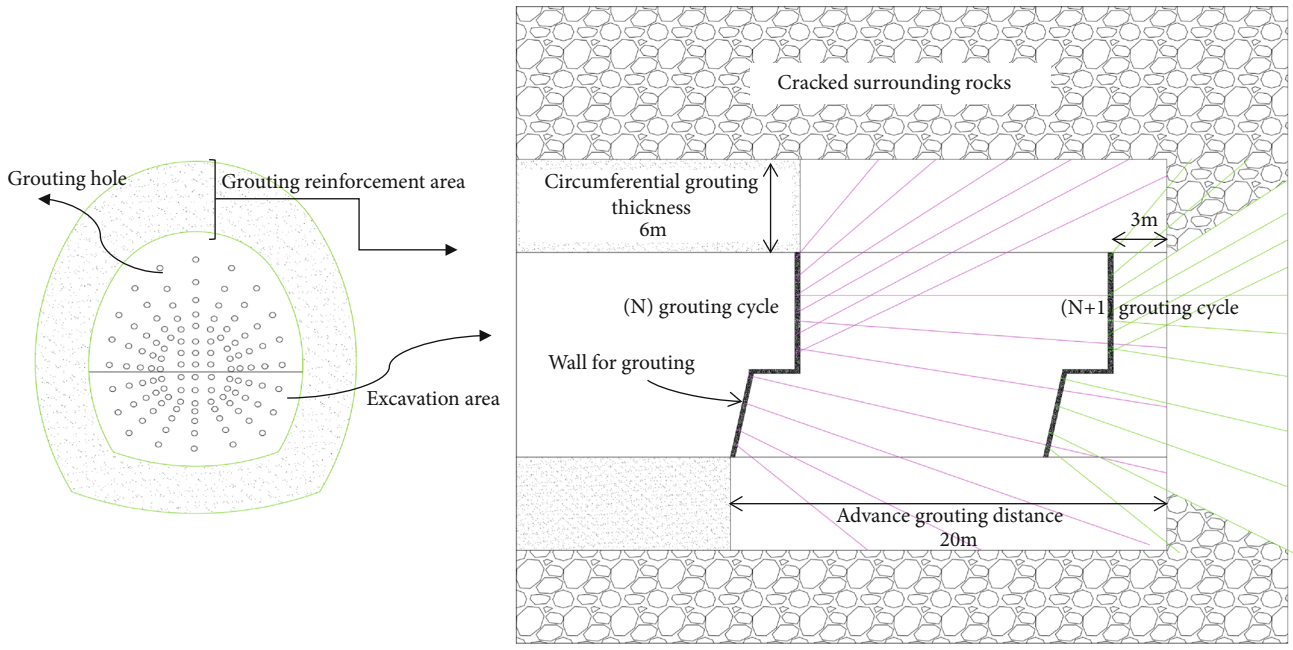

Figure 9: Design of curtain grouting.

As shown in Figure 9, the large-section advanced curtain grouting in the broken zone and water rich section of the tunnel is 6 m beyond the tunnel excavation contour. The effective diffusion radius of single-hole grouting is 3.6 m. The center distance of grouting hole bottom is 15 m, and the grouting pressure is 1.7 MPa. The grouting length is 20 m, and 3 m is reserved for excavation after each grouting section is completed. The thickness of grout stop wall is 20 cm. The grouting material is cement water glass double slurry. The fineness modulus of sodium silicate is 2.4~3.4, the concentration is 35° B é, and the volume ratio of cement and water glass is 3 : 1. Disodium hydrogen phosphate was used as retarder, and its content was 2~2.5% of the weight of sodium silicate. Figure 10 shows the actual implementation of the project.

After grouting, the water inflow was measured by drilling, and most of the holes were basically without water, as shown in Figure 11. The water yield of the hole with the largest water inflow was 0.2 L/min, which met the requirement of

(a) (b)

Figure 10: Project implementation. (a) Wall for grouting. (b) Grouting reinforcement.

Figure 11: Probe hole after grouting.

water inflow less than 0.3 L/min. From the perspective of excavation. The stability of the tunnel face is obviously improved, and the excavation process is smooth. After grouting in the whole face, the slurry diffuses in the rock stratum in a dendritic manner, the permeability of surrounding rock decreases, and the water inflow decreases from about 7500 m^3/day to 1300 m^3/day, which has a significant decrease.

5. Conclusion

In this paper, the mechanism of water inrush in water rich stratum and the optimization scheme of curtain grouting parameters are taken as the main research object, and the water and mud inrush disaster of Jingzhai tunnel is taken as the engineering support. Through geological exploration, theoretical analysis, numerical calculation, and other research methods, combined with engineering application, the mechanism of tunnel mud and water inrush under the influence of excavation disturbance is deeply carried out. The development law of tunnel cracks under different grouting parameters is analyzed, and the beneficial conclusions with certain theoretical value and engineering significance are obtained.

(1) Through the magnetotelluric method, the distribution range of the water rich area of the tunnel is obtained. There is a large range of fault fracture zone near the fault, and the water source in the fracture zone is rich

(2) The parameters of grouting are determined by numerical simulation. The development law of tunnel surrounding rock crack under different curtain grouting parameters is studied. When the grouting thickness is less than 3 m, the cracks will run through the grouting area. According to the analysis, the thickness of curtain circumferential grouting should be 5-7 m. The advance influence range of the tunnel caused by excavation is 2-3 m, so 3 m advance grouting protection area is selected

(3) When the curtain thickness is 3 M, the tunnel water inflow has two processes: incubation and explosion. When the curtain thickness is 5 m and 7 m, the appearance of water gushing is obviously improved, and the gushing process shows three stages: incubation, growth, and stability. According to the results of numerical simulation, the grouting thickness is 6 m, the advance grouting range is 20 m, and the slurry is cement water glass double slurry. The actual situation shows that the grouting scheme can effectively restrain the water gushing from the tunnel

Data Availability

The data used to support the findings of this study are available from the corresponding author upon request.

Conflicts of Interest

The authors declare that they have no conflicts of interest.

Acknowledgments

This work was supported in part by the Research on Intelligent Construction Method and Technical System of Sichuan Tibet Railway, based on active control of surrounding rock deformation (P2019G038).

References

[1] J. Shao, F. Zhou, and W. Sun, "Evolution model of seepage characteristics in the process of water inrush in faults," *Geofluids*, vol. 2019, Article ID 4926768, 14 pages, 2019.

[2] W. Sun, Y. Xue, T. Li, and W. Liu, "Multi-field coupling of water inrush channel formation in a deep mine with a buried fault," *Mine Water and the Environment*, vol. 38, no. 3, pp. 528–535, 2019.

[3] W. Liu, J. Zhao, R. Nie, Y. Liu, and Y. du, "A coupled thermal-hydraulic-mechanical nonlinear model for fault water inrush," *Processes*, vol. 6, no. 8, p. 120, 2018.

[4] Q. Zhou, J. Herrera, and A. Hidalgo, "The numerical analysis of fault-induced mine water inrush using the extended finite element method and fracture mechanics," *Mine Water and the Environment*, vol. 37, no. 1, pp. 185–195, 2018.

[5] X. Wang, C. Liu, S. Chen, L. Chen, K. Li, and N. Liu, "Impact of coal sector's de-capacity policy on coal price," *Applied Energy*, vol. 265, article 114802, 2020.

[6] X. Hu, L. Wang, Y. Lu, and M. Yu, "Analysis of insidious fault activation and water inrush from the mining floor," *International Journal of Mining Science and Technology*, vol. 24, no. 4, pp. 477–483, 2014.

[7] Z. Li, H. Liu, Z. Dun, L. Ren, and J. Fang, "Grouting effect on rock fracture using shear and seepage assessment," *Construction and Building Materials*, vol. 242, article 118131, 2020.

[8] Q. Wu, Y. Liu, D. Liu, and W. Zhou, "Prediction of floor water inrush: the application of GIS-based AHP vulnerable index

method to Donghuantuo coal mine, China," *Rock Mechanics and Rock Engineering*, vol. 44, no. 5, pp. 591–600, 2011.

[9] Q. Wu, H. Xu, and W. Pang, "GIS and ANN coupling model: an innovative approach to evaluate vulnerability of karst water inrush in coalmines of North China," *Environmental Geology*, vol. 54, no. 5, pp. 937–943, 2008.

[10] Z. Li, S. Liu, W. Ren, J. Fang, Q. Zhu, and Z. Dun, "Multiscale laboratory study and numerical analysis of water-weakening effect on shale," *Advances in Materials Science and Engineering*, vol. 2020, Article ID 5263431, 2020.

[11] Z. Li, H. Zhou, D. Hu, and C. Zhang, "Yield criterion for rock-like geomaterials based on strain energy and CMP model," *International Journal of Geomechanics*, vol. 20, no. 3, article 04020013, 2020.

[12] Q. Meng, H. Wang, M. Cai, W. Xu, X. Zhuang, and T. Rabczuk, "Three-dimensional mesoscale computational modeling of soil-rock mixtures with concave particles," *Engineering Geology*, vol. 277, article 105802, 2020.

[13] B. Li and W. Qiang, "Catastrophic evolution of water inrush from a water-rich fault in front of roadway development: a case study of the Hongcai coal mine," *Mine Water and the Environment*, vol. 38, no. 2, pp. 421–430, 2019.

[14] S. Liu, W. Liu, and D. Yin, "Numerical simulation of the lagging water inrush process from insidious fault in coal seam floor," *Geotechnical and Geological Engineering*, vol. 35, no. 3, pp. 1013–1021, 2017.

[15] X. Zhang, Y. Wu, E. Zhai, and P. Ye, "Coupling analysis of the heat-water dynamics and frozen depth in a seasonally frozen zone," *Journal of Hydrology*, no. article 125603, 2020.

[16] C. Zhu, M. C. He, M. Karakus, X. B. Cui, and Z. G. Tao, "Investigating toppling failure mechanism of anti-dip layered slope due to excavation by physical modelling," *Rock Mechanics and Rock Engineering*, vol. 53, no. 11, pp. 5029–5050, 2020.

[17] J. Liu, W. Chen, J. Yuan, C. Li, Q. Zhang, and X. Li, "Groundwater control and curtain grouting for tunnel construction in completely weathered granite," *Bulletin of Engineering Geology and the Environment*, vol. 77, no. 2, pp. 515–531, 2018.

[18] S. Li, R. Liu, Q. Zhang, and X. Zhang, "Protection against water or mud inrush in tunnels by grouting: a review," *Journal of Rock Mechanics and Geotechnical Engineering*, vol. 8, no. 5, pp. 753–766, 2016.

[19] X. Zhang, S. Li, Q. S. Zhang et al., "Study of key-hole grouting method to harness high pressure water gushing in fractured rock mass," *Chinese Journal of Rock Mechanics and Engineering*, vol. 30, no. 7, pp. 1414–1421, 2011.

[20] H.-m. Jiang, L. Li, X.-l. Rong, M.-y. Wang, Y.-p. Xia, and Z.-c. Zhang, "Model test to investigate waterproof-resistant slab minimum safety thickness for water inrush geohazards," *Tunnelling and Underground Space Technology*, vol. 62, pp. 35–42, 2017.

[21] Q. Liu, S. Chen, S. Wang, J. Chai, and D. Zhang, "Experimental development process of a new cement and gypsum-cemented similar material considering the effect of moisture," *Geofluids*, vol. 2020, Article ID 8831801, 14 pages, 2020.

[22] S. Saleh, N. Z. M. Yunus, K. Ahmad, and N. Ali, "Improving the strength of weak soil using polyurethane grouts: a review," *Construction and Building Materials*, vol. 202, pp. 738–752, 2019.

[23] Y. Liang, W. Sui, and J. Qi, "Experimental investigation on chemical grouting of inclined fracture to control sand and water flow," *Tunnelling and Underground Space Technology*, vol. 83, pp. 82–90, 2019.

[24] Z. Xu, C. Liu, X. Zhou, G. Gao, and X. Feng, "Full-scale physical modelling of fissure grouting in deep underground rocks," *Tunnelling and Underground Space Technology*, vol. 89, pp. 249–261, 2019.

[25] P. Yang, Y.-h. Liu, S.-w. Gao, and Z.-c. Li, "Experiment on sealing efficiency of carbon fiber composite grout under flowing conditions," *Construction and Building Materials*, vol. 182, pp. 43–51, 2018.

[26] X. Li, L. Wang, M. Hao, Y. Zhong, and B. Zhang, "An analytical solution for the radial flow of variable density grout in rock fractures," *Construction and Building Materials*, vol. 206, pp. 630–640, 2019.

[27] Y.-H. Liu, P. Yang, Z.-B. Ouyang, X. Wei, and L. Zhang, "Effect of Nano-CaCO 3 on the sealing efficiency of grouts in flowing water grouting," *KSCE Journal of Civil Engineering*, vol. 24, no. 10, pp. 2923–2930, 2020.

[28] L. Zou, U. Håkansson, and V. Cvetkovic, "Yield-power-law fluid propagation in water-saturated fracture networks with application to rock grouting," *Tunnelling and Underground Space Technology*, vol. 95, article 103170, 2020.

[29] E. Eberhardt, "The Hoek–Brown failure criterion," *Rock Mechanics and Rock Engineering*, vol. 45, no. 6, pp. 981–988, 2012.

[30] J. Clausen and L. Damkilde, "An exact implementation of the Hoek-Brown criterion for elasto-plastic finite element calculations," *International Journal of Rock Mechanics and Mining Sciences*, vol. 45, no. 6, pp. 831–847, 2008.

[31] X. Zheng, R. Zhang, and Q. Wang, "Comparison and analysis of two Coulomb friction models on the dynamic behavior of slider-crank mechanism with a revolute clearance joint," *Applied Mathematics and Mechanics*, vol. 39, no. 9, pp. 1239–1258, 2018.

[32] T. Yona and Y. Or, "The wheeled three-link snake model: singularities in nonholonomic constraints and stick–slip hybrid dynamics induced by Coulomb friction," *Nonlinear Dynamics*, vol. 95, no. 3, pp. 2307–2324, 2019.